Spectrochimica Acta Part A: Molecular and Biomolecular Spectroscopy 97 (2012) 762–770

Contents lists available at SciVerse ScienceDirect

Spectrochimica Acta Part A: Molecular and Biomolecular Spectroscopy

journal homepage: www.elsevier.com/locate/saa

Design, synthesis and DNA binding activities of late first row transition metal(II) complexes of bi- functional tri – and tetratopic imines

Priya P. Netalkar, Anupama Kamath, Sandeep P. Netalkar, Vidyanand K. Revankar *

Department of Studies in Chemistry, Karnatak University, Pavate Nagar, Dharwad 580 003, Karnataka, India

HIGHLIGHTS

- Series of tri and tetratopic complexes of bi-functional imines have been prepared.
- Metal complexes exhibit enhanced antibacterial activity compared to ligands.
- Ligands and their complexes bind to DNA via intercalative mode of interaction.

GRAPHICAL ABSTRACT

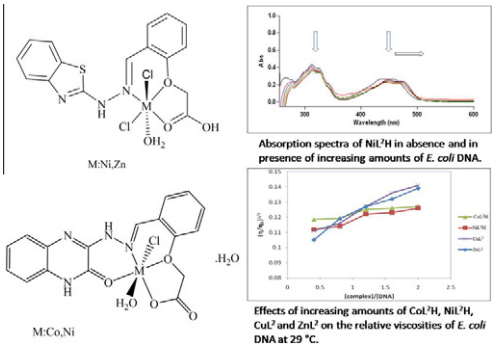

ARTICLE INFO

Article history:
Received 10 April 2012
Received in revised form 12 July 2012
Accepted 13 July 2012
Available online 24 July 2012

Keywords:
Benzothiazole
2-Hydroxy-3-hydrazinebenzopyrazine
2-Formylphenoxyacetic acid
Antimicrobial activity
DNA binding study

ABSTRACT

A series of novel Co(II), Ni(II), Cu(II) and Zn(II) complexes of tri and tetratopic hydrazones have been prepared. Ligands L^1H_2 and L^2H_2 were synthesized by the condensation of 2-formylphenoxyacetic acid with 2-hydrazinobenzothiazole and 2-hydroxy-3-hydrazinebenzopyrazine, respectively. The prepared complexes were characterized by the analytical and spectral techniques. All the complexes were found to be monomeric in nature with octahedral geometry. Both ligands were found to be electrochemically active in the working potential range showing single electron transfer process attributed to the deprotonation of carboxylic group of the 2-formylphenoxyacetic acid. The potency of the ligand and its complexes as antimicrobial agents has been investigated and made to interact with *Escherichia coli* DNA to investigate the binding/cleaving ability by absorption, hydrodynamic and electrophoresis studies.

Introduction

Schiff base metal complexes of multidentate aromatic ligands have been of current interest in the field of medicinal research and in development of new therapeutic agents, mainly due to the fact that they exhibit novel electronic and/or magnetic properties with fascinating structural features, as well as the ability of these ligands to be modulated to DNA binding and cleaving abilities [1–3]. Basically, metal complexes interact with double helix DNA in either non-covalent or covalent way. The former way includes three binding modes, i.e., intercalation, groove binding and external static electronic effects. Among these, intercalation is being one of the most important. The intercalating ability is known to increase with the planarity of ligands [4]. Additionally, the coordination geometry and nature of donor atom play key roles in determining the binding extent of the complexes to DNA. Lastly, the importance of the central metal ion at the core of the structure of the DNA binding molecule is noteworthy [5,6]. Many DNA interactive heterocyclic compounds, including benzothiazole and benzopyrazine derivatives, have already been evaluated and have found to be efficient DNA intercalators [7,8].

* Corresponding author. Tel.: +91 9900485652/+91 836 4250821 (Res.).
E-mail address: vkrevankar@rediffmail.com (V.K. Revankar).

1386-1425/$ - see front matter © 2012 Elsevier B.V. All rights reserved.
http://dx.doi.org/10.1016/j.saa.2012.07.066

2-Formylphenoxyacetic acid, in combination with benzothiazole/benzopyrazine derivatives facilitates the formation of tri- and tetradentate metal complexes with N and O donor ligand system with labile anion in the coordination sphere. The presence of labile chloride in complexes is an interesting thing in this study as they allow the binding of the metal centre with N-7 of purine bases after deprotonation. Furthermore, the coordination model of the above ligands affords a greater choice and flexibility involving the N (azomethine nitrogen, ring nitrogen of benzothiazole) and O (ethereal oxygen, carboxylate oxygen, hydroxyl group of benzopyrazine). In the present paper, we report the preparation and characterization of transition metal(II) complexes of tri and tetratopic Schiff base ligands and their interactions with *Escherichia coli* DNA.

Experimental

Reagents and apparatus

All chemicals were of reagent grade and solvents were distilled and dried before use according to the standard procedures. 2-Formylphenoxyacetic acid [9], 2-hydrazino benzothiazole [10], and 2-hydroxy-3-hydrazinebenzopyrazine [11] were prepared according to the standard procedures reported elsewhere. The zinc chloride used was anhydrous whereas the other metal salts were in their hydrated form, i.e., $CoCl_2{\cdot}6H_2O$, $NiCl_2{\cdot}6H_2O$ and $CuCl_2{\cdot}2H_2O$. Estimation of the metal(II) ions were done according to the standard methods. The molar conductivity measurements were made on ELICO-CM-82 conductivity bridge. The magnetic susceptibility measurements were made on Faraday balance at room temperature using $Hg[Co(SCN)_4]$ as calibrant. The ^1H NMR spectra were recorded in DMSO-d_6 solvent on Bruker-300 MHz spectrometer at room temperature using TMS as internal reference. IR spectra were recorded in a KBr matrix using an Impact-410 Nicolet (USA) FT-IR spectrometer in 4000–400 cm^{-1} range. The electronic spectra of the complexes were recorded on a Hitachi 150–20 spectrophotometer in the range of 1000–200 nm. The cyclic voltametric studies were performed at room temperature in DMSO under O_2 free condition using CH instruments Electrochemical analyzer, CHI-1110A (USA). The ESR spectra of the copper complexes were scanned on a Varian E-4X-band EPR spectrometer, using TCNE as the g-marker. TG and DTA measurements of the complexes were recorded in nitrogen atmosphere on Universal V2. 4F TA instrument keeping final temperature at 800 °C and heating rate was 10 °C/min. The FAB mass spectra were drawn from JEOL SX 102/DA-6000 mass spectrometer using Argon/Xenon (6 kV, 10 mA) as the FAB gas.

Syntheses

Preparation of the ligands L^1H_2 and L^2H_2

The ethanolic solution of 2-hydrazinobenzothiazole (3.3 g; 0.02 mol) and 2-hydroxy-3-hydrazinebenzopyrazine (3.54 g; 0.02 mol) was added slowly to 2-formylphenoxyacetic acid (3.6 g; 0.02 mol) in ethanol with constant stirring to form L^1H_2 (Scheme 1) and L^2H_2 (Scheme 2), respectively. Catalytic amount of glacial acetic acid was added to the solution and the homogeneous reaction mixture was refluxed on water bath for 3 h. The pale yellow solid that formed upon cooling, was filtered off and recrystallized from hot ethanol. (L^1H_2: M.P. 285–287 °C, Yield: 70%; L^2H_2: M.P. 230–232 °C, Yield: 65%).

Preparation of complexes

To a stirred ethanolic solution (50 ml) of respective metal chlorides, viz, Co(II), Ni(II), Cu(II), and Zn(II) chloride (0.005 mol), an ethanolic solution of ligand (0.005 mol) was added and stirred for about 15 min, further the reaction mixture was refluxed on water bath for 4 h. So obtained solids were filtered, washed with hot ethanol and dried over fused $CaCl_2$. The proposed structures of the complexes are given in Scheme 3.

Methodology for DNA binding/cleavage analysis

The concentration of *E. Coli* DNA per nucleotide [C(p)] was measured by using its known extinction coefficient at 260 nm, 600 M^{-1} cm^{-1}. The absorbance of the DNA at 260 nm (A260) and 280 nm (A280) were measured to check its purity. The ratio A260/A280 was 1.84, indicating that the DNA was satisfactorily free from protein [12]. Buffer (5 mM tris(hydroxymethyl) aminomethane, pH 7.2, 50 mM EDTA) was used for the absorption, viscosity and thermal denaturation experiments.

Absorption studies

In the spectroscopic absorption studies, the complex was dissolved in DMSO to get the desired concentration. The spectroscopic titrations were carried out by adding increasing amounts (20, 40, 60, 80 and 100 μl) of DNA to a solution of the complex (2 ml) at a fixed concentration contained in a quartz cell, UV–Vis spectra were recorded after equilibration at 23 °C for 10 min after each addition. The intrinsic binding constant K_b was determined from the plot of $A_0/[A - A_0]$ versus $[DNA]^{-1}$ according to Eq. (1) [13].

$$Ao/[A - Ao] = \varepsilon_G/[\varepsilon_{E-H} - \varepsilon_G] + \varepsilon_G/[\varepsilon_{E-H} - \varepsilon_G] \times 1/K[DNA] \quad (1)$$

where A_0 and A are the absorbance observed for MLCT absorption band for the free complex and absorbance observed for MLCT absorption band at given DNA concentration, respectively. [DNA] is the concentration of DNA in base pairs, ε_G and ε_{H-G} are the apparent absorption coefficients in free and DNA bounded form of complex, respectively. The data were fitted into the above equation to obtain a graph, with a slope equal to $\varepsilon_G/[\varepsilon_{E-H}-\varepsilon_G] \times 1/K$ and intercept equal to $\varepsilon_G/[\varepsilon_{E-H}-\varepsilon_G]$ hence K_b was obtained from the ratio of the intercept to the slope.

Viscosity measurements

DNA binding studies using viscosity measurements were carried out using an Oswald micro-viscometer, maintained at constant temperature (29 °C) with a thermostat. The DNA concentration was kept constant in all samples, but the complex concentration was increased each time (from 50 to 250 mM). Mixing of the solution was achieved by bubbling nitrogen gas through the viscometer. The mixture was left for 10 min at 23 °C after addition of each aliquot of complex. The flow time was measured with a digital stopwatch. The experiment was repeated in triplicate. Data are presented as $(\eta/\eta_0)^{1/3}$ versus the ratio [complex]/[DNA], where η and η_0 are the specific viscosity of DNA in presence and in absence of the complex, respectively. The values of η and η_0 were calculated using Eq. (2),

$$\tau = (t - t_b)/t_b \quad (2)$$

where t_b is the observed flow time of DNA containing solution and t is the flow time of buffer alone. Relative viscosities for DNA were calculated from the relation (η/η_0) [14].

Electrophoresis

For the gel electrophoresis experiments [15], the solution of complexes in DMF (1 mg/mL) was prepared and these test samples (1 μg) were added to the genomic DNA samples of *E. Coli* and incubated for 2 h at 37 °C. Agarose gel was prepared in TAE buffer (4.84 g Tris base, PH 8.0, 0.5 M EDTA/lL. PH 7.3), the solidified gel attained at ~55 °C was placed in electrophoresis chamber flooded with TAE buffer. After that 20 μL of each of the incubated complex-DNA mixtures (mixed with bromophenol blue dye at 1:1 ratio) was

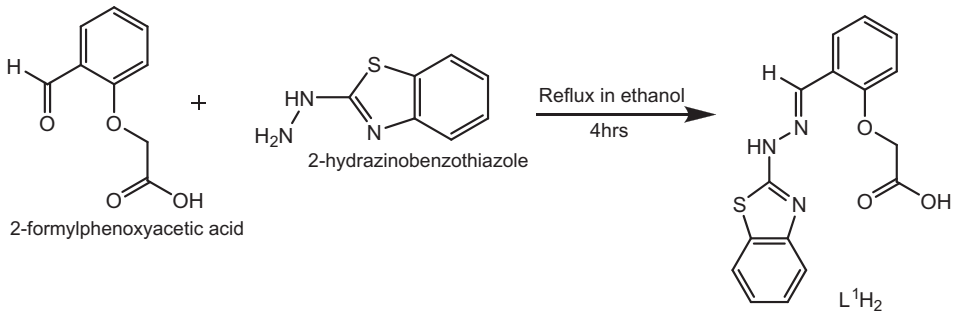

Scheme 1. Schematic representation of synthesis of L^1H_2.

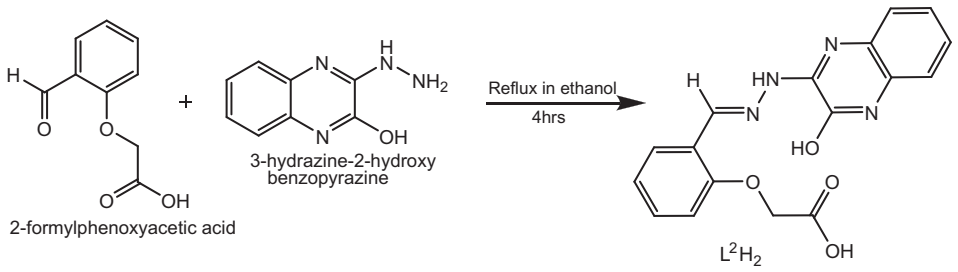

Scheme 2. Schematic representation of synthesis of L^2H_2.

loaded on the gel along with standard DNA marker and electrophoresis was carried out under TAE buffer system at 50 V for 2 h. At the end of electrophoresis, the gel was carefully stained with EtBr (ethidiumbromide) solution (10 μg/mL) for 10–15 min and visualized under UV light using a Bio-Rad Trans illuminator. The illuminated gel was photographed by using a Polaroid camera (a red filter and Polaroid film were used).

Results and discussion

The analytical and physicochemical data of the complexes are summarized in Table 1. All complexes are soluble in organic solvents like DMF, DMSO and acetonitrile.

Infrared spectral studies

Infrared frequencies for the ligands and complexes along with their assignments are presented in Table 2. Ligand L^1H_2 show a carboxylic carbonyl group frequency at 1714 cm^{-1}, which decreases by 5–10 cm^{-1} in all the complexes, except in Co(II) complex, indicating the involvement of carbonyl oxygen in coordination. In Co(II) complex, coordination occurred through carboxylic –OH after deprotonation. The ν(C=N) appears at 1612 cm^{-1} as an intense sharp peak in the ligand, show negative shift in case of Ni(II) and Zn(II) whereas positive shift in case of Co(II) and Cu(II) complexes [16], indicating the coordination of azomethine nitrogen [17]. The ν(C=N) of benzothiazole ring observed at 1575 cm^{-1} show positive shift in case of Co(II) indicating coordination through ring nitrogen whereas in the case of Ni(II) and Zn(II) complexes, the band remain unaltered suggesting the nonparticipation of ring nitrogen in the coordination. On the other hand, in case of Cu(II) complex, a new band has appeared at 1654 cm^{-1} attributed to exo-azomethine group formed at second position of the benzothiazole ring due to the tautomerization. In this case coordination has occurred through ring nitrogen. Asymmetric stretching of C–O–C in the ligand is assigned in the frequency range of 1292 cm^{-1}, which shifts to lower energy side in complexes, implying the coordination of ethereal oxygen. The low frequency bands in all the complexes in the region 500–470 cm^{-1} and 400–325 cm^{-1} are assigned to ν(M–N) and ν(M–O), respectively. The ligand shows a broad medium intensity band at 3202 cm^{-1} which can be assigned to the ν(NH),which experiences a little shift upon complexation. Non-involvement of sulfur of the benzothiazole in coordination is assumed in all these complexes, which is in accordance with earlier reports [18] on the benzothiazole complexes with various transition metal ions, this is because the sulfur is a poor Lewis base compared to nitrogen in the benzothiazole.

Ligand L^2H_2 shows a carboxylic carbonyl group frequency in the region of 1690 cm^{-1}, which remains almost same in the all the complexes, suggesting non-involvement of carbonyl oxygen atom in coordination. Further a weak band around 3429 cm^{-1} in ligand is assigned to –OH stretching frequency. It is difficult to account for the coordination of oxygen of the –OH via deprotonation as all the complexes shows a strong broad band in the region 3400 cm^{-1} due to water molecule. The new sharp band at 1682 and 1669 cm^{-1} in case of Co(II) and Ni(II) complexes, respectively assigned to ν(C=O) of amide functionality which is absent in the free ligand suggesting amido-imidol tautomerism [19]. But in the case of Cu(II) and Zn(II) complexes imidol tautomer is retained as in case of free ligand and coordination through oxygen via deprotonation is seen. Asymmetric stretching of C–O–C in the ligand is assigned in the frequency range of 1296 cm^{-1}, which shifts to lower energy side in complexes, implying the coordination of ethereal oxygen. The ν(C=N) of azomethine group appears at 1653 cm^{-1} as an intense sharp peak in the ligand, shifts to a lower frequency side by about 15–20 cm^{-1} in complexes, suggesting the coordination of azomethine nitrogen. The ligand shows a broad medium intensity band at 3276 cm^{-1} which can be assigned to the ν(NH), which experiences a little shift upon complexation. The low frequency bands in all the complexes in the region 500–470 cm^{-1} and 400–325 cm^{-1} are assigned to ν(M–N) and ν(M–O), respectively.

^{1}H NMR spectral studies

The Ligand L^1H_2 is scanned in the range 0–16 ppm for ^{1}H NMR studies. Within this range it display singlets at 12.6, 8.4, 7.9 ppm,

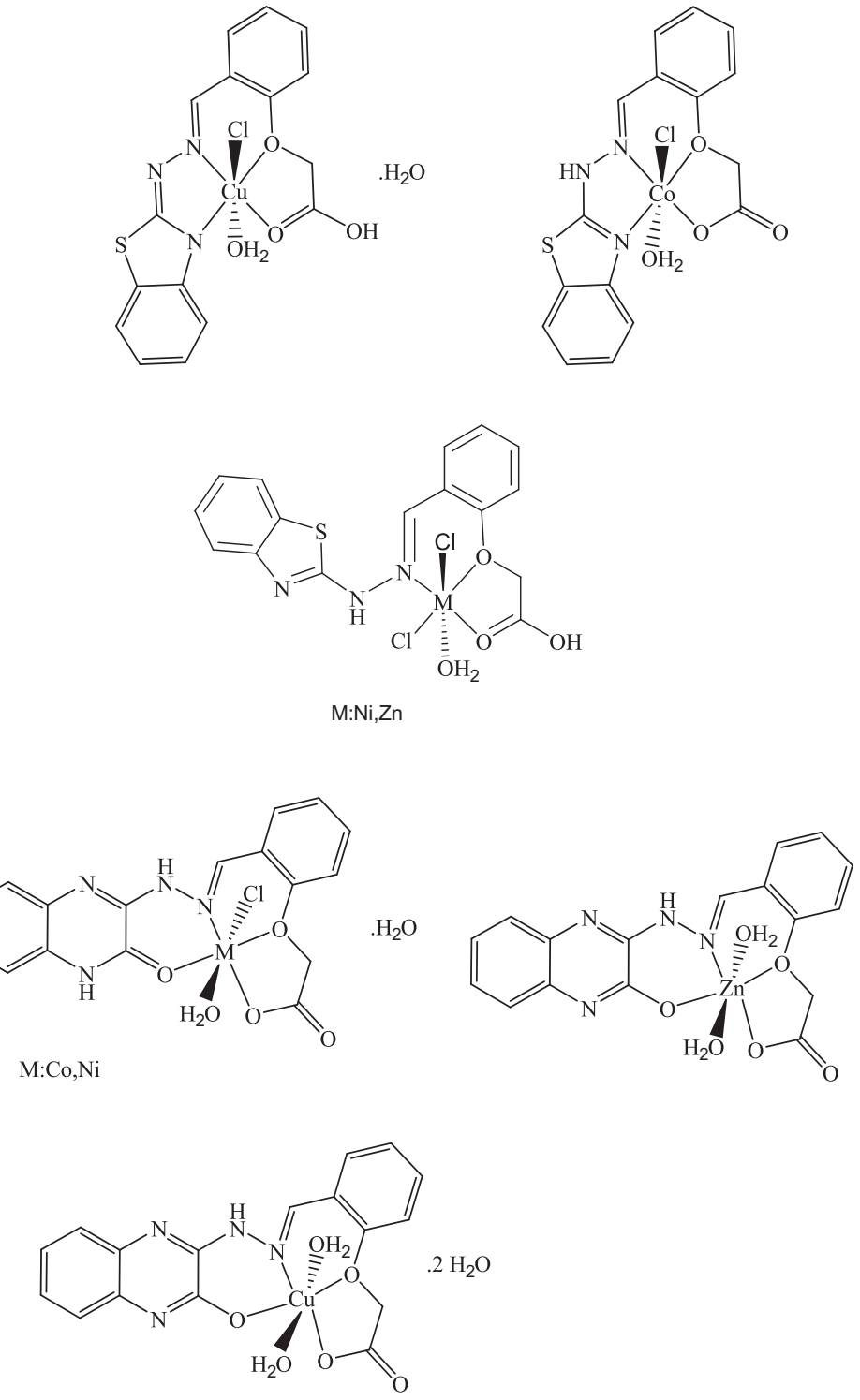

Scheme 3. Tentative structures of complexes.

which are attributed to carboxylic –OH (1H) (D_2O exchangeable) azomethine proton (1H), and –NH proton, respectively and a multiplet in the range 6.9–7.8 ppm which are assigned to aromatic protons. In addition to these prominent peaks, a singlet observed at 4.8 ppm is assigned to methylene protons of the ethereal linkage. In contrast, its zinc complex shows a downfield shift of carboxylic –OH at 12.79 ppm, azomethine proton at 8.7 ppm, methylene protons of the ethereal linkage at 4.9 ppm, confirms the coordination through azomethine nitrogen, carbonyl oxygen and ethereal oxygen. The peak due to –NH proton does not suffer any change in complex implying its non-involvement in coordination.

The ^{1}H NMR spectrum of the ligand L^2H_2 shows the singlets at 12.3 and 11.3 ppm due to carboxylic –OH (1H) and aromatic –OH (D_2O exchangeable) of quinoxaline moiety respectively. Both the peaks disappeared in the zinc complex, indicating their involvement in coordination to the metal ion via deprotonation. The singlets observed at 8.9 and 7.9 ppm in the spectrum of ligand are

Table 1
Analytical, conductivity data of the ligand L^1H_2, L^2H_2 and their complexes.

Compound	Emprical formula	Elemental analysis (%) calculated (found)					Molar cond. ΛM ohm^{-1} cm^2 mol^{-1}	Magnetic moment in $\mu_{eff.}$ BM
		C	H	N	M	Cl		
L^1H_2	$C_{16}H_{13}N_3O_3S$	58.71 (57.7)	3.97 (3.4)	12.84 (12.2)	–	–		–
CoL^1H	$[Co(C_{16}H_{12}N_3O_3S)Cl{\cdot}H_2O]$	43.60 (42.8)	3.63 (3.5)	9.58 (9.32)	13.37 (13.2)	8.05 (8.15)	12.74	4.83
NiL^1H_2	$[Ni(C_{16}H_{13}N_3O_3S)Cl_2{\cdot}H_2O]$	40.59 (41.1)	3.17 (2.6)	8.87 (8.96)	13.53 (12.4)	14.70 (15.1)	13.31	2.87
CuL^1H	$[Cu(C_{16}H_{12}N_3O_3S)Cl{\cdot}H_2O]{\cdot}H_2O$	41.60 (43.4)	3.50 (3.0)	9.11 (10.0)	13.77 (14.3)	7.68 (7.88)	17.12	1.80
ZnL^1H_2	$[Zn(C_{16}H_{13}N_3O_3S)Cl_2{\cdot}H_2O]$	41.26 (41.4)	3.22 (3.1)	(9.02) (9.00)	14.05 (14.1)	15.23 (15.1)	12.30	Diamagnetic
L^2H_2	$C_{17}H_{14}O_4N_4$	60.35 (60.7)	4.17 (4.2)	16.56 (15.8)	–	–		–
CoL^2H	$[Co(C_{17}H_{13}N_4O_4)(Cl)(H_2O)]{\cdot}H_2O$	43.64 (44.1)	3.68 (3.5)	11.98 (11.5)	12.60 (12.7)	7.59 (7.45)	7.29	4.68
NiL^2H	$[Ni(C_{17}H_{13}N_4O_4)(Cl)(H_2O)]{\cdot}H_2O$	43.64 (43.3)	3.69 (3.4)	11.98 (12.2)	12.56 (12.3)	7.60 (7.54)	14.69	2.92
CuL^2	$[Cu(C_{17}H_{12}N_4O_4)(H_2O)_2]{\cdot}2H_2O$	43.31 (43.2)	4.24 (4.3)	11.88 (11.6)	13.46 (13.3)	–	8.47	1.82
ZnL^2	$[Zn(C_{17}H_{12}N_4O_4)(H_2O)_2]$	46.64 (43.7)	3.68 (3.6)	12.80 (12.1)	14.94 (14.6)	–	14.33	Diamagnetic

assigned to the –NH and azomethine proton, respectively and a multiplet in the range 6.9–7.9 ppm is due to aromatic protons, shows a small shift in the spectrum of zinc complex. Methylene protons attached to ethereal linkage shows a singlet at 4.7 ppm, exhibited a downfield shift at 4.9 ppm in the complex indicating involvement of ethereal oxygen in coordination. Hence the ligand coordinates through carboxylic oxygen, enolic oxygen and azomethine nitrogen to the metal ion.

Molar conductivity measurements

The molar conductance values of the complexes in DMSO at 10^{-3} M concentration are in the range of 7–18 mho^{-1} cm^2 mole (Table 1), much less than that expected for 1: 1 electrolytes [20], hence all complexes are considered as non-electrolytes.

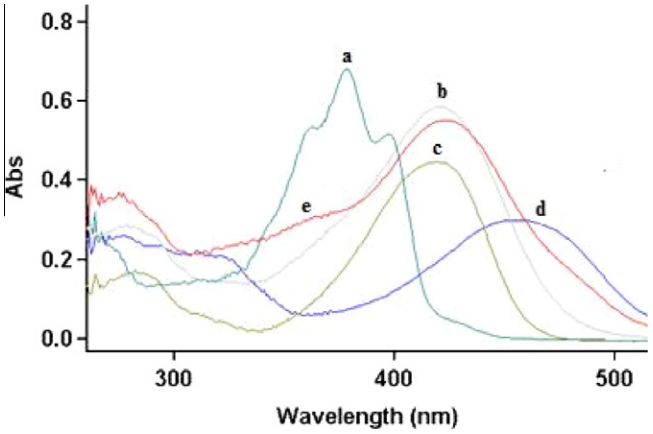

Fig. 1. UV–visible spectra of ligand and its complexes in the range 250–500 nm. (a) L^1H_2, (b) CoL^1H, (c) NiL^1H_2, (d) CuL^1H, (e) ZnL^1H_2.

Electronic spectral studies

Electronic absorption spectra of all the compounds were recorded in DMSO solution over the range 200–1000 nm. Absorption spectra of L^1H_2 and its complexes are shown in Fig. 1. L^1H_2 and L^1H_2 shows bands at 280 and 276 nm corresponding to π–π^* transition whereas the peak at 397 and 308 nm corresponds to n–π^* transition associated with azomethine linkage respectively [21]. These bands have suffered red shift upon complexation indicating the coordination of azomethine group. Electronic spectrum of CoL^1H shows a medium-intensity band at 424 nm assignable to charge transfer transition and well-resolved, low-intensity band at 600 nm assignable to $^4T_{1g}(F) \rightarrow {}^4A_{2g}(P)$ transition [22]. CoL^2H exhibits a charge transfer broad band around 470 nm and $^4T_{1g}(F) \rightarrow {}^4T_{1g}(P)$ transition is obscured into it. NiL^1H_2 complex exhibits bands at 680 nm $[^3A_{2g} \rightarrow {}^3T_{1g}(F)]$ and 530 nm $[^3A_{2g} \rightarrow {}^3T_{1g}(P)]$ corresponding to d–d transitions and charge transfer transition is observed at 423 nm. The electronic spectrum of NiL^2H shows a charge transfer band at 430 nm. The low intensity

Table 2
IR spectral data (cm^{-1}) of the ligand L^1H_2, L^2H_2 and their complexes.

Compound	ν(OH)	ν(NH)	ν(C=O)	ν(C=O) Amidic	ν(C=N)	–O–CH2–
L^1H_2	3538	3202	1714	–	1612	1292s
CoL^1H	3428	3150(sh)	1708	–	1618	1275
NiL^1H_2	3460	3293	1633	–	1590(sh)	1289
CuL^1H	3432	3112	1687	–	1617	1287
ZnL^1H_2	3427	3062	1639	–	1604	1281
L^2H_2	3429	3276	1690	–	1653	1296(sh)
CoL^2H	3552	3157	1687	1682	1640	1283
NiL^2H	3330	3196	1689	1669	1639	1290
CuL^2	3426	3157	1691	–	1620	1280(sh)
ZnL^2	3430	2923	1691	–	1646	1285

bands at 850, 560 and 470 nm are assignable to $^3A_{2g} \rightarrow {}^3T_{2g}(F)$, $^3A_{2g} \rightarrow {}^3T_{1g}(F)$ and $^3A_{2g} \rightarrow {}^3T_{1g}(P)$ transitions, respectively (Supplementary Figure-S1), collectively all these offers the octahedral geometry for the nickel complex [23]. Electronic spectrum of CuL^1H complex exhibits the broad band in the region 380–500 nm due to charge transfer transition and very low intensity band at 750 nm assignable to $^2E_g \rightarrow {}^2T_{2g}$ (d–d) transition (Supplementary Figure-S2 (a)). In Case of CuL^2 broad band in the region 400–450 and 679 nm are assignable to the charge transfer transition and $^2E_g \rightarrow {}^2T_{2g}$ (Supplementary Figure-S2 (b)) which is in agreement with the octahedral geometry of copper complexes. Finally, both the Zn (II) complexes shows charge transfer bands at around 350–430 nm.

Magnetic susceptibility measurements

The magnetic moments measured at room temperature are listed in Table 1. The electronic spectral data and the observed magnetic moments for the cobalt, nickel and copper complexes of both the ligands suggest the existence of octahedral geometry around metal ions. The magnetic moment values for CoL^1H and CoL^2H were found to be 4.83 and 4.68 BM [24], for NiL^1H_2 and NiL^2H, 2.87 and 2.92 BM [25] and for CuL^1H and CuL^2 values found were 1.80 and 1.82 BM, respectively, slightly higher than the spin-only value which may be due to the spin orbit coupling [26].

ESR spectral studies

The powder state X-band ESR spectra of copper complexes were operated in the region of 9000 MHz with corresponding field intensity at 3000 Gauss in powder state at room temperature. Both CuL^1H and CuL^2 complexes exhibit isotropic intense broad signal with g_{iso} 2.072 and 2.081, respectively with no hyperfine splitting [27]. Broad ESR signal may be due to bulkier ligand around the metal ion [28].

FAB mass spectral studies

The FAB mass spectrum of copper complexes was recorded by using m-NO_2 benzyl alcohol as matrix. FAB mass spectra of CuL^1H and CuL^2 complexes show molecular ion peak corresponding to m/z at 443 and 435, respectively, consistent with monomeric nature of complexes. Apart from this, spectra show some other peaks, which are due to molecular ions of various fragments of the complexes. By comparing all the analytical and spectral data of cobalt, nickel and zinc complexes, it is evident that all complexes are monomeric.

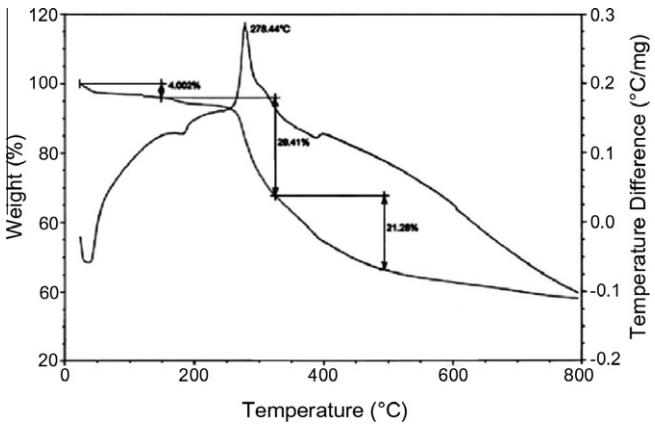

Fig. 2. TG–DTA spectrum of CuL^1H.

Table 3
Cyclic voltammetric data of ligand L^1H_2, L^2H_2 and their copper complexes.

Complex	Scan rate (V/s)	E_{pc} (V)	E_{pa} (V)	ΔE_p (V)	$E_{1/2}$ (V)
L^1H_2	0.1	0.1	0.05	0.05	0.075
CuL^1H	0.1	−0.35	0.6	0.09	0.125
L^2H_2	0.05	−0.2	0.15	0.15	−0.025
CuL^2	0.05	0.0	0.55	0.05	0.275

*$\Delta E_p = E_{pa} - E_{pc}$; $E_{1/2} = [E_{pc} + E_{pa}]/2$.

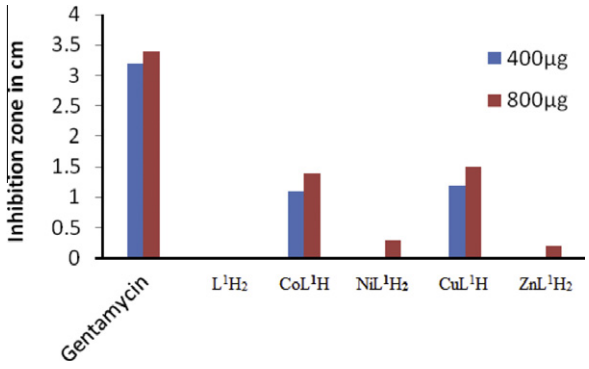

Fig. 3a. Graphical representation of antibacterial analysis of L^1H_2 and its complexes.

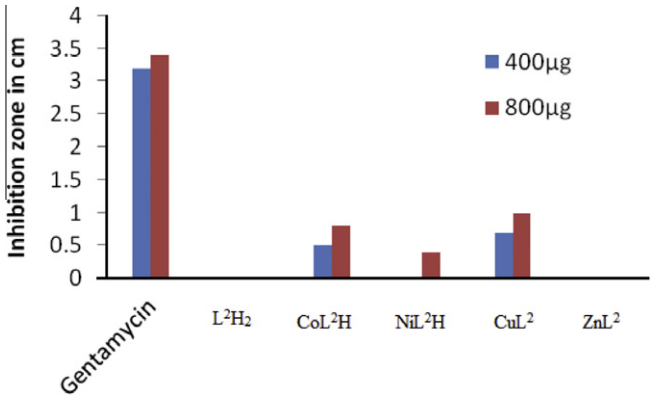

Fig. 3b. Graphical representation of antibacterial analysis of L^2H_2 and its complexes.

Thermal study

The thermogravimetric analyses of all the complexes have been carried out in nitrogen environment over the temperature range of 30–800 °C. The TG/DTA analysis of CuL^1H is used as representative example (Fig. 2). TG–DTA curves of CuL^1H show weight losses in three considerable stages. In the first stage around 8.0%, in the temperature range 35–250 °C is attributed to the weight loss of one coordinated water molecule along with one lattice held water molecule, which is further supported by the endothermic signal in DTA. Further weight loss in the region 250–325 °C is attributed to the loss of one chloride along with the ligand and in the final part degradation of remaining ligand has been observed. Finally the graph became plateau because of the formation of stable metal oxide.

Similarly, TG–DTA curves of CuL^2 show weight losses in three considerable stages. In the first stage 7.9%, in the temperature range 55–160 °C is attributed to the weight loss of two lattice held water molecules, which is further supported by the DTA peak at

108 °C. In the next step the weight loss around 8% is attributed to two coordinated water molecules. Further weight loss in the temperature range 350–600 °C is attributed to the loss of ligand to form stable metal oxide. TG–DTA graphs of cobalt, nickel and zinc complexes follow the same pattern with slight differences.

Cyclic voltammetric studies

The cyclic voltammograms were scanned in the potential range of −1.0 to +1.0 V with scan rates 0.05, 0.1, and 0.15 Vs^{-1} in DMSO under oxygen free conditions and data are summarized in Table 3. The cyclic voltammograms of L^1H_2 and CuL^1H complex are used as representative examples in Supplementary material (Figure-S3(a) and Figure-S3(b)). Both the ligands were found to be electrochemically active in the working potential range showing single electron transfer process, an anodic peak was observed at 0.05 and 0.15 V, respectively. In the reverse scan, the cathodic peak was observed at 0.1 and −0.2 V, respectively. This spectacular behavior of both the ligands in the working potential range is attributed to the deprotonation of carboxylic group of the 2-formylphenoxyacetic acid [29,30] (Supplementary Figure-S4). The separation between anodic and cathodic peak potentials (ΔEp) is 50 and 150 mV, respectively indicating a reversible and quasireversible redox process for both electroactive ligands supported by Ipc/Ipa ≈1 values. The cyclic voltammograms of both Cu(II) complexes show a single electron transfer process, an anodic peak was observed at 0.6 and 0.55 V, respectively. In the reverse scan, the cathodic peak was observed at −0.35 and 0.0 V, respectively. The separation between anodic and cathodic peak potentials (ΔEp) is 95 and 55 mV, respectively indicating a quasireversible and reversible redox process for both electroactive copper complexes supported by Ipc/Ipa values which are nearly equal to 1.

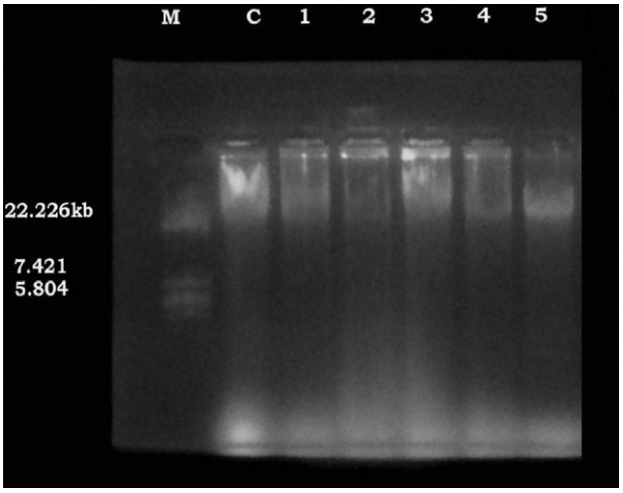

Fig. 4a. Gel electrophoresis pictures of ligand L^1H_2 and their complexes. Photograph showing the effects of transition metal complexes on DNA of *E. coli*. Lane M: DNA marker, Lane C: Untreated DNA, Lane 1: L^1H_2, Lane 2: CoL^1H, Lane 3: NiL^1H_2, Lane 4: CuL^1H, Lane 5: ZnL^1H_2.

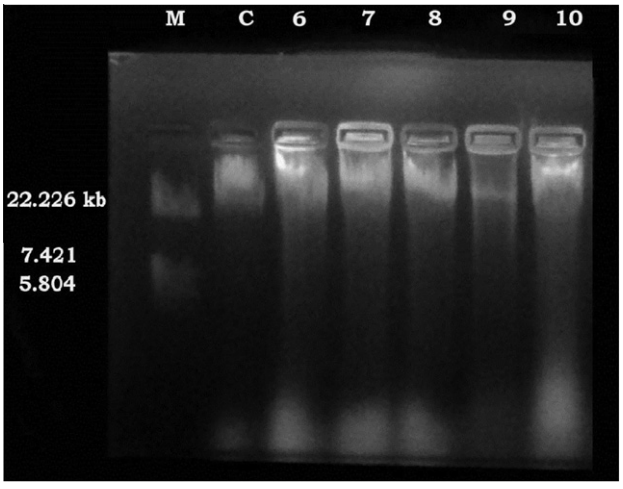

Fig. 4b. Gel electrophoresis pictures of ligand L^2H and their complexes. Photograph showing the effects of transition metal complexes on DNA of *E. coli*. Lane M: DNA marker, Lane C: Untreated DNA, Lane 6: L^2H, Lane 7: CoL^2H, Lane 8: NiL^2H, Lane 9: CuL^2, Lane 10: ZnL^2.

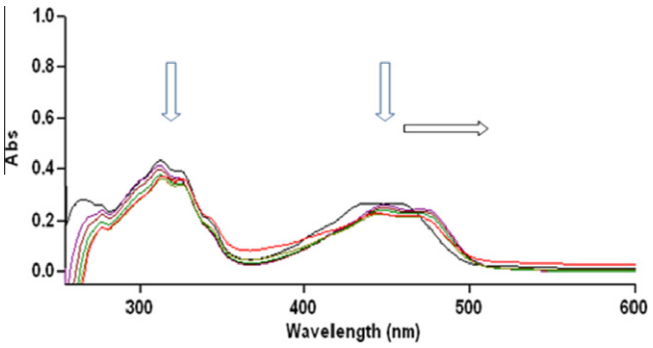

Fig. 5. Absorption spectra of NiL^2H in absence (very first line from pinnacle) and in presence of increasing amounts of *E. coli* DNA. Arrow mark shows the absorption changes upon changing the *E. coli* DNA concentration.

Table 4
Intrinsic binding constants of the complexes.

Sl No.	Complex	K_b
1	CoL^1H	1.43×10^4
2	NiL^1H_2	2.2×10^4
3	CuL^1H	4.3×10^4
4	ZnL^1H_2	1.3×10^4
5	CoL^2H	1.5×10^4
6	NiL^2H	1.9×10^4
7	CuL^2	1.03×10^5
8	ZnL^2	1.9×10^4

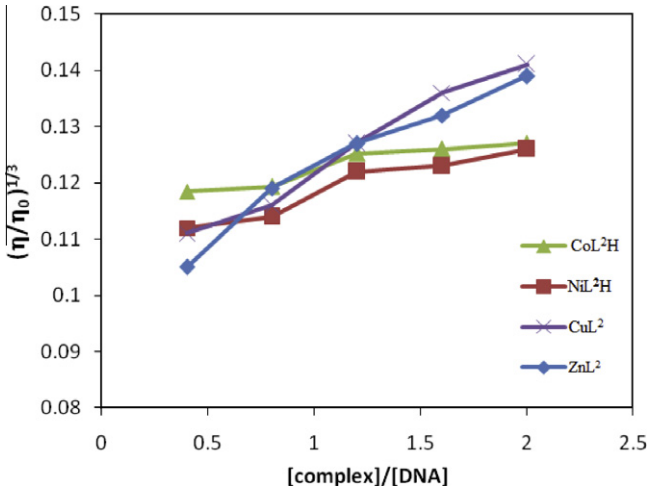

Fig. 6. Effects of increasing amounts of CoL^2H, NiL^2H, CuL^2 and ZnL^2 on the relative viscosities of *E. coli* DNA at 29 °C.

Biochemistry

Anti-biogram analysis

In order to study the comparative biological activities, the compounds were screened for antibacterial (against *E. coli*) in the range 25–800 mg concentrations. From the antibacterial studies it is inferred, that both the ligands were found to be inactive against *E. coli*. The results obtained are graphically represented in Figs. 3a and b. From the graph it is clear that there is enhancement in the inhibitory activity of the complexes, which is represented by the high degree of activity in case of copper and cobalt complexes derived from L^1H_2, whereas, in the case of L^2H_2, moderate activity has been showed by both these complexes. All the other complexes were found to be less active against the bacterium tested. Inhibitory activities of metal complexes against bacterial species have enhanced as compared to the ligand indicating that complexation is able to modulate or alter antibacterial property.

DNA cleavage studies by gel-electrophoresis method

The interactions between the free ligand and complexes with DNA are shown in Figs. 4a and b. Gel-electrophoresis technique works on the migration of DNA under the influence of electric potential. The photograph shows the bands with different bandwidth, compared to the control, is the differentiating criteria for binding ability of complexes with *E. coli* in this study. Control experiment using DNA alone does not show any significant cleavage of DNA even after a longer exposure time. In the photograph Fig. 4a, untreated DNA (lane c) is more intense and has slightly bigger width compared to the bands of free ligand L^1H_2 and the complexes except lane 3 NiL^1H_2. This result could be attributed to the interaction of DNA to a small extent for L^1H_2 and its complexes except NiL^1H_2. On the other hand, in Fig. 4b, lane 9, corresponding to CuL^2 shows decrease in intensity and bandwidth indicating the interaction of complex with DNA whereas L^2H_2 and its complexes shows no significant changes in the intensity and bandwidth compared to the control. We conclude from the gel electrophoresis studies that there is no significant cleavage of DNA by the action of either free ligands or its complexes.

DNA binding analysis using electronic spectral method

The DNA binding characteristics of the complexes have been studied by UV–visible spectral studies, keeping the complex at fixed concentration and varying the concentration of DNA solution. If the binding involves a typical intercalative mode, an effect of hypochromism coupled with bathochromism for the characteristic peaks of the small molecules will be found due to the strong stacking between the chromophore and the base pairs of DNA. The extent of the hypochromism commonly parallels the level of the intercalation. The absorption spectra of the complex NiL^2H in the absence and presence of different concentrations of DNA are illustrated in Fig. 5. The spectrum of the representative complex NiL^2H shows three maxima at around 320 and 430 nm, characteristic of the $n-\pi^*$ and charge transfer transition of the complex with d–d transition at around 470 nm. Addition of DNA in increasing amounts to the complex causes slight hypochromism in the charge transfer transitions, whereas for the absorption peak at 470 nm, slight hypochromism with bathochromic shift (~5 nm) was seen which demonstrated that complex probably bind to DNA via an intercalative mode [31]. For the remaining complexes, hypochromism is observed in both the d–d and charge transfer regions with a substantial red shift, indicating the intercalative mode of binding of the complexes to the DNA. The binding constants (K_b) of the complexes are given in Table 4.

DNA binding analysis using viscosity measurement

Hydrodynamic (viscosity) measurements are sensitive to changes in the length of DNA base pairs and are regarded as the least ambiguous and the most critical tests of a binding model in solution in the absence of crystallographic structural data. Intercalative binding is confirmed by the lengthening of the DNA helix as base pairs are separated to accommodate the binding compound, leading to an increase in viscosity of DNA solution [14,32]. The present complexes show such an increase, suggesting an intercalative binding to DNA as shown in Fig. 6.

Conclusion

It is concluded from the analytical and spectral data that these ligands act as tri and tetradentate chelates with N_2O_2, NO_2 and NO_3 donating sites. The Ligand L^2H_2 and its complexes show amido-imidol tautomerism. All the complexes are found to be octahedral and monomeric in nature. Cyclic voltammograms of ligands and its copper complexes show single electron transfer process. The metal complexes have higher antimicrobial activity than the ligand, especially Co(II) and Cu(II) complexes. Spectroscopic studies together with viscosity experiments support that, both the ligands and their complexes bind to DNA via intercalative mode of interaction whereas no significant cleavage of DNA have been observed.

Acknowledgments

The authors thank the USIC and Department of chemistry, Karnatak University, Dharwad for providing spectral facility. Recording of FAB mass spectra (CDRI Lucknow) and ESR spectra (IIT Bombay) are gratefully acknowledged. The authors thank UGC for providing RFSMS and DST for INSPIRE fellowship.

Appendix A. Supplementary data

Supplementary data associated with this article can be found, in the online version, at http://dx.doi.org/10.1016/j.saa.2012.07.066.

References

[1] F. Liang, P. Wang, X. Zhou, T. Li, Z.Y. Li, H.K. Lin, D.Z. Gao, C.Y. Zheng, C.T. Wu, Bioorg. Med. Chem. Lett. 14 (2004) 1901–1917.
[2] C. Metcalfe, J.A. Thomas, Chem. Soc. Rev. 32 (2003) 215–224.
[3] S. Arturo, B. Giampaolo, R. Giuseppe, L.G. Maria, T. Salvatore, J. Inorg. Biochem. 98 (2004) 589–594.
[4] H. Xu, K.C. Zheng, H. Deng, L.J. Lin, Q.L. Zhang, L.N. Ji, Dalton Trans. 3 (2003) 2260–2268.
[5] H. Zhang, C.S. Liu, X.H. Bu, M. Yang, J. Inorg. Biochem. 99 (2005) 1119–1125.
[6] J.K. Barton, Pure Appl. Chem. 61 (1989) 563–564.
[7] G.S. Kurdekar, M.P. Sathisha, N.V. Kulkarni, S. Budagumpi, V.K. Revankar, Med. Chem. Res. 20 (2011) 421–429.
[8] W. Szczepanik, M. Kucharczyk-Klaminska, P. Stefanowicz, A. Staszewska, Z. Szewczuk, J. Skała, A. Mysiak, M. Jezowska-Bojczuk, Bioinorg. Chem. Appl. 2009 (2009) 1–10.
[9] B.S. Furniss, A.J. Hannaford, P.W.G. Smith, A.R. Tatchell, fifth ed. Vogel's Textbook of Practical Organic Chemistry, 2007.
[10] (a) V.K. Revankar, V.H. Arali, V.B. Mahale, Indian J. Chem. 29A (1990) 889–894; (b) A. Rutavicius, S. Iokubaitite, Khim. Geterutsikl Soedin. 1 (1984) 40.
[11] S.M. Annigeri, M.P. Sathisha, V.K. Revankar, Trans. Met. Chem. 32 (2007) 81–87.
[12] S. Zhang, Y. Zhu, C. Tu, H. Wei, Z. Yang, L. Lin, J. Ding, J. Zhang, Z. Guo, J. Inorg. Biochem. 98 (2004) 2099–2103.
[13] X.J. Dang, M.Y. Nie, J. Tong, H.L. Li, J. Electroanal. Chem. 448 (1998) 61–67.
[14] S. Satyanarayana, J.C. Dabrowiak, J.B. Chaires, Biochemistry 31 (1992) 9319–9324.
[15] A. Arslantas, A.K. Devrim, H. Necefoglu, Int. J. Mol. Sci. 8 (2007) 564–571.
[16] D.M. Wiles, T. Suprunchuk, Can. J. Chem. 47 (1969) 1087–1089.
[17] C.N.R. Rao, Chemical Application of Infrared Spectroscopy, Academic press, New York, 1963.
[18] J.C. Thompson Rendell, L.K. Thompson, Can. J. Chem. 57 (1979) 1–7.
[19] L. Sacconi, Coord. Chem. Rev. 1 (1966) 126–132.

[20] W.J. Geary, Coord. Chem. Rev. 7 (1971) 81–122.
[21] N.V. Kulkarni, G.S. Hegde, G.S. Kurdekar, S. Budagumpi, M.P. Sathisha, V.K. Revankar, Spectrosc. Lett. 43 (2010) 1–12.
[22] (a) H. Olmez, F. Arslan, H. Icbudak, J. Therm. Anal. Calorim. 76 (2004) 793–800;
(b) N.V. Kulkarni, M.P. Sathisha, S. Budagumpi, G.S. Kurdekar, V.K. Revankar, J. Coord. Chem. 63 (2010) 1451–1461.
[23] A.B.P. Lever, Inorganic Electronic Spectroscopy, Elsevier, Amsterdam, The Netherlands, 1984.
[24] Z.M. Zaki, G.G. Mohamed, Spectrochim. Acta 56 (2000) 1245–1250.
[25] B.N. Figgs, J. Lewis, Modern Coordination Chemistry Intensience, New York, 1967.
[26] S.M. Annigeri, A.D. Naik, U.B. Gandadharmath, V.K. Revankar, V.B. Mahale, Trans. Met. Chem. 27 (2002) 316–320.
[27] N. Raman, S. Ravichandran, C. Thangaraja, J. Chem. Sci. 116 (2004) 215–219.
[28] A.L. Ram, B. Debajani, K.D. Arjun, K. Arvind, Trans. Met. Chem. 32 (2007) 481–493.
[29] S.K. Mandal, L.K. Thompson, M.J. Newlands, F.L. Lee, Y. Lepage, J.P. Charland, E.J. Gabe, J. Inorg. Chim. Acta 122 (1986) 199–205.
[30] B.R. Eggins, J.Q. Chambers, J. Eletrochem. Soc. 89 (1967) 3910–3913.
[31] S. Khan, S.A.A. Nami, K.S. Siddiqi, E. Husain, I. Naseem, Spectrochim. Acta Part A 72 (2009) 421–428.
[32] S. Satyanarayana, J.C. Daborusak, J.B. Chaires, Biochemistry 32 (1993) 2573–2584.